EES Catalysis

COMMUNICATION

View Article Online
View Journal | View Issue

Cite this: *EES Catal.*, 2026, 4, 77

Received 13th August 2025,
Accepted 14th October 2025

DOI: 10.1039/d5ey00246j

rsc.li/eescatalysis

Thin-film $Cu_{1-x}N_x$ catalysts for efficient CO_2 reduction: a scalable magnetron sputtering approach

Mathias van der Veer, [ab] Nick Daems, [a] Pegie Cool [b] and Tom Breugelmans *[a]

Thin-film-based catalysts, fabricated through physical vapor deposition, have attracted significant interest as promising materials for electrochemical CO_2 reduction. In this context, metallic Cu films function as active catalyst layers for the reduction to ethylene and ethanol. However, these films still experience high overpotentials, resulting in low energy efficiencies. In this study, we have fabricated $Cu_{1-x}N_x$ films to overcome this issue by incorporating nitrogen into the sputtering process, leading to the formation of an anti-ReO_3 crystal structure of Cu_3N, which contains interstitial vacancies filled with Cu atoms. Under optimal sputtering conditions of r_{N2} = 0.50, sputter rate = 4 Å s^{-1}, and pressure = 6 μbar, EDX analysis reveals a sub-stoichiometric thin-film composed of $Cu_{0.84}N_{0.16}$. In the electrochemical CO_2 reduction, this film resulted in an increase in energy efficiency from 15.8% to 20% for ethylene compared to pure Cu films, which was attributed to a decrease in the measured potential by ± 500 mV, due to the addition of nitrogen in the structure. This key finding suggests that for future applications, $Cu_{1-x}N_x$ layers should be employed instead of metallic Cu to reduce the required energy demands while maintaining selectivity.

Broader context

As the field of CO_2 capture and utilization is increasing, many believe that the electrochemical CO_2 reduction holds a future as a large-scale industrial application of efficiently using CO_2 as a feedstock to produce valuable chemicals such as CO, Formic acid, Ethylene, and Ethanol. Driven by renewable electricity, efficient catalysts are needed. In literature, metallic Cu films are widely used to study large-scale operation of CO_2 reduction. However, we note that Cu_3N films, synthesized by adding N_2 to the sputter process, are more efficient catalysts and reduce the energy requirements. Especially since the formation of Ethylene and Ethanol require 12 e^- per mole, the energy demands are quite high. Therefore, reducing overpotentials is a key area that is sometimes overlooked. Herein, we highlight an increase of 25% in energy efficiency and a 20% increase in mass activity by simply changing the cathode material to Cu_3N. Furthermore, initial stability was also improved, due to the strong presence of N^{3-}, which maintains the presence of Cu^+, and thus reduces catalysts reconstructions that can be detrimental to the operational process. These reasons led us to believe that future research should be conducted with Cu_3N films.

Introduction

Extreme weather events have become the new norm as increasing anthropogenic emissions of CO_2 and other greenhouse gases over the past few decades have contributed to rising global temperatures.[1] In this context, researchers worldwide have focused on the electrochemical CO_2 reduction reaction (eCO_2R), which has emerged as a promising strategy to mitigate the increased CO_2 levels in the atmosphere. This technique can be powered by sustainable energy sources, and thus has the potential to convert wasteful CO_2 into valuable chemicals such as ethylene, ethanol, CO, and formic acid, which help to close the carbon cycle. An efficient electrocatalyst is required to produce certain products with high faradaic efficiency (FE), low energy input, high stability (>10 000 h), and high production rates to make it commercially viable and competitive with more traditional fossil fuel based routes. Among the wide variety of CO_2 products, C_{2+} products are more desirable than

[a] *Applied Electrochemistry and Catalysis (ELCAT), University of Antwerp, Campus Drie Eiken, Universiteitsplein 1, 2610, Wilrijk, Belgium. E-mail: Tom.breugelmans@uantwerpen.be*
[b] *Laboratory of Adsorption and Catalysis (LADCA), University of Antwerp, Campus Drie Eiken, Universiteitsplein 1, 2610, Wilrijk, Belgium*

C_1 due to their high energy density and commercial value.[2] However, the reaction to ethylene and ethanol is challenging due to the multiple proton-coupled electron transfers required, resulting in diverse reaction pathways and, thus in most cases, a poor selectivity.[3–6]

Cu-based catalysts, such as Cu[7]/Cu_2O[8–10] or Cu–M (M = Ag,[11–13] Pd,[14] Zn,[15] Bi[16]) are known to synthesize C_{2+} products albeit with high energy input, relatively poor stability, and low selectivity towards a single product. Recently, a flow cell design has been reported for the conversion of CO_2 to ethylene, with a FE reaching up to 70%, and a remarkable stability of 150 h, nevertheless this was only achieved with highly corrosive alkaline electrolytes (>7 M KOH).[17] As a result, tuning Cu-catalysts for more efficient production of a single multi-carbon product at less demanding conditions remains of paramount importance to advance the field. In this regard, Cu_3N catalysts are promising as the limited research into them has shown higher ethylene efficiencies but so far only in H-cell conditions and thus at low current densities. For instance, a study conducted by Yin *et al.*, synthesized Cu_3N nanocubes through wet chemical synthesis as electrocatalysts for CO_2 to ethylene with a reported FE of 60%.[18] Similarly, Wang *et al.* synthesized Cu_3N nanoparticles enclosed with (100) and (111) facets, which operated at a high FE of 61%.[19] Finally, Cu_3N-derived Cu nanowires proposed by Mi *et al.* showed a total C_{2+} of 86% with ethylene being the main product at 66%, and a high stability of 28 h.[20] From these results, it is clear that Cu_3N has a catalytic capability towards ethylene, with a more narrow product selectivity than typical Cu/Cu_2O catalysts but they need to be evaluated under the more industrially relevant conditions of a flow cell and high current densities.[8,9,10,21,22] The main challenge with Cu-based catalysts is the *in situ* reduction of the active Cu^+ species, which leads to surface reconstructions and subsequent loss of activity.[2,21] Sargent *et al.* suggested that Cu_3N could prolong the stability of the copper(I) species, which are known to aid in decreasing energy barriers for *CO adsorption and subsequent C–C coupling.[22] Moreover, the above mentioned catalyst designs are often complex and require specific chemicals that may be toxic or costly, which also limits their scalability. For this reason, other ways to synthesize these Cu_3N materials are required if they are to replace the typical CuO_x catalysts also in flow electrolyzers.

In this respect, a promising route towards the preparation of stable $Cu_{1-x}N_x$ films on which abundant research has been performed is the physico-chemical fabrication approach including methods such as atomic layer deposition,[23] reactive radio-frequency sputtering,[24] and direct current magnetron sputtering,[25] resulting in the application of this metastable semiconductor Cu_3N in various fields such as photovoltaics,[26] optical storage devices,[23] H_2 gas sensing,[27] and tunnel junctions[28] but as of yet Cu_3N-based films prepared by this approach have not found their way to eCO_2R. As a non-toxic, and earth-abundant material, it can nevertheless be a viable alternative to other toxic materials. Direct current (DC) sputtering stands out as it provides high scalability, improved homogeneity, controllable thickness and crystallinity.

In this study, we have fabricated Cu-based thin films with reactive sputtering, by adding nitrogen to the argon flow, resulting in the formation of $Cu_{1-x}N_x$ sub stoichiometric layers. By controlling different operational parameters such as N_2/Ar gas fraction (r_{N2}), deposition pressure (P), and sputter rate (Å s^{-1}), we found an optimal sub-stoichiometric layer of $Cu_{0.84}N_{0.16}$ for the eCO_2R to increase the energy efficiency towards ethylene compared to typical metallic Cu thin film. We have thus proven that the implementation of nitrogen in traditional Cu-based thin films can significantly decrease the energy consumption, which is an important discovery, especially for future up scaling research.

Results

Physiochemical results

$Cu_{1-x}N_x$ films were deposited onto carbon-based gas diffusion layers (GDLs), and the influence of operational pressure (P), sputter deposition rate (SR), and nitrogen ratio (r_{N2}) on the total Cu deposition and the performance of the eCO_2R was studied towards C_{2+} products, such as ethylene and ethanol. Various physicochemical characterizations, such as ICP-MS, XRD, SEM, and contact angle, are provided to gain insight in those parameters that have the largest impact on performance. All experimental methods, including the synthesis, characterizations methods, and eCO_2R experiments are explained in detail in the supporting information. Table S1 summarizes the synthesis conditions of all fabricated thin – films, along with the ICP-MS results to determine the Cu loading.

A gradual increase in r_{N2} lowered the total Cu deposition. Because N is a lighter atom than Ar, it has a lower intrinsic kinetic energy, and thus, it yields a slower material transfer rate.[23,24,29,30] However, during DC magnetron sputtering, the reactive gas (N_2) can be implemented into the subsurface region of the Cu target. Nitrogen can remain as non – reactive ions in the target or form an insulating layer, this results in an increase in power and a decrease of the target erosion rate.[31] In other words, the bombardment of the Cu target was less effective, resulting in decreased deposition rates.

Next, an increase in sputter pressure also results in reduced deposition, as evidenced by the lower Cu loadings. This was explained as follows in a study by Figueira *et al.*,[29] as the atoms in the plasma undergo an increased number of collisions, the mean free path and thus the chances of reaching the target are reduced, along with more target poisoning due to an increase of nitrogen during sputtering, as such decreasing the total deposition.[32]

Finally, a higher initial sputtering rate results in more power being applied during operation (see Table S1); and therefore, more localized target heating occurs, which increases the kinetic energy of the Cu atoms, leading to more evaporation.[33] Furthermore, a more efficient cleaning of the target also occurs, which helps in reducing the target poisoning. Ultimately, both results in a higher loading.

To identify the crystalline phases, the XRD patterns of the different films were obtained. A distinct peak in all samples was

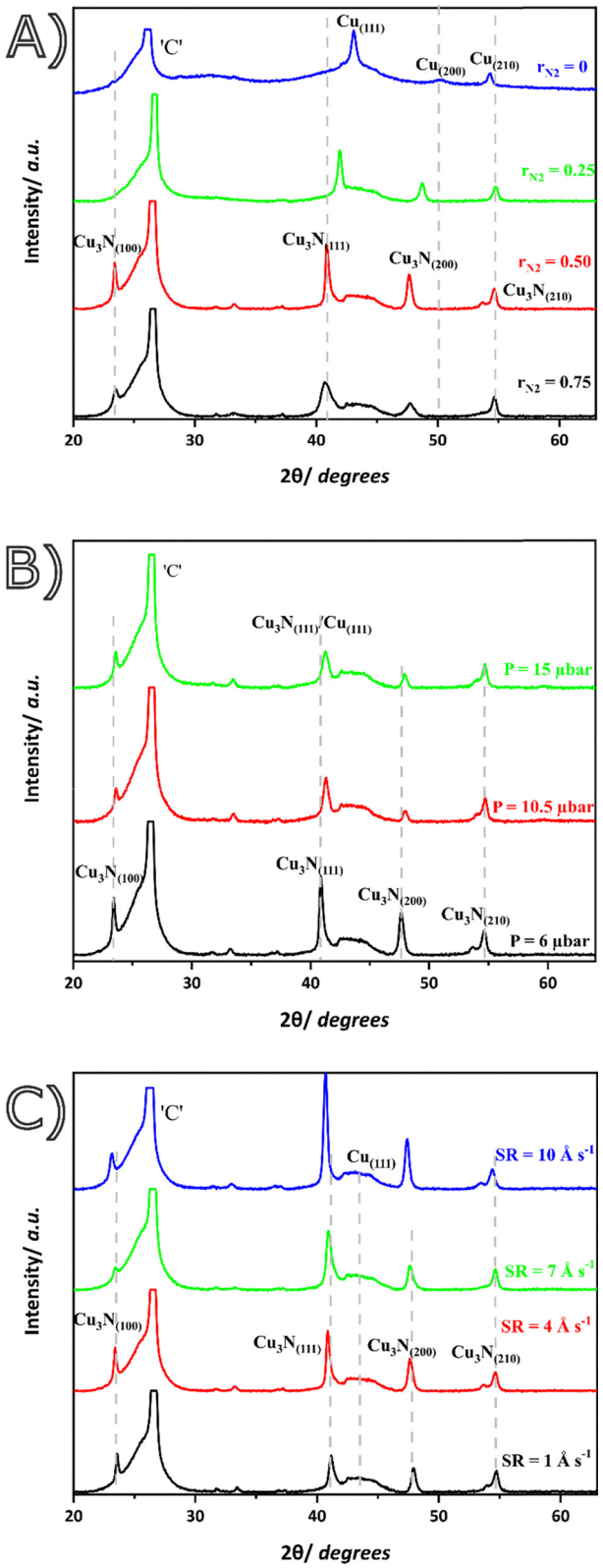

Fig. 1 XRD patterns of the different prepared samples. (A) $Cu_{1-x}N_x$ with varying r_{N2}, constant operational pressure at 6 µbar and sputter rate of 4 Å s^{-1}. (B) $Cu_{1-x}N_x$ with varying pressure, constant r_{N2} = 0.50, and sputter rate of 4 Å s^{-1} (C) $Cu_{1-x}N_x$ with varying sputter rate constant r_{N2} = 0.50, and constant operational pressure at 6 µbar. The phases and indices are labelled.

identified at 28° corresponding to the carbon substrate, which is henceforth labelled 'C'. The peak potential value has been restricted to increase sensitivity of the important peaks. To identify the remaining peaks, reference patterns for Cu_3N (JCPDS File No. 47-1088) and Cu (JCPDS File No. 04-0836) were used. Fig. 1 presents the XRD patterns for all prepared samples. In Fig. 1A, the influence of r_{N2} is evident. For r_{N2} = 0, diffraction peaks corresponding to metallic Cu appear at 43° (111), 50° (200), and 53° (210), while no Cu_3N peaks are observed. Upon increasing the r_{N2} factor, characteristic Cu_3N peaks emerge at 23° (100), 41° (111), 47° (200), and 54° (210). Simultaneously, the Cu peaks gradually shift toward those of Cu_3N, reflecting the growth of Cu_3N domains.[24,25,30] Nevertheless, residual Cu remain detectable, likely due to the formation of sub-stoichiometric layers in which Cu may exist as interstitial atoms or separate Cu domains. Furthermore, SEM–EDX images (Fig. S2) revealed that an increase in r_{N2} caused the particles to change from distinct spherical particles to more stacked agglomerated platelets, with sharp edges.[24] EDX subsequently determined the percentage of N present in the sample, for increasing r value, this was respectively, 0–13–16–21% (Table S1).

Next, the influence of sputter pressure was investigated in Fig. 1B. The effect of sputter pressure on the crystallinity has been well reported in the literature:[34–37] a low pressure (<6 µbar) results in grains that grow along the Cu_{111} plane,[37] which favors creation of more sub-stoichiometric layers due to a low reactive character of the sputtering process.

A higher operating pressure (15 µbar) will shorten the mean free path, and more atomic collisions will thus occur. As a consequence, the kinetic energy of the Cu species arriving at the substrate will be lower than at lower pressures (6 µbar). The Cu ions with lower energy will be deposited with a more amorphous character, as they lack energy to organize in ordered structures. Upon increasing the pressure, the Cu_3N peaks that are visible at 6 µbar are less intense and shifted towards metallic Cu peaks, evident of a more amorphous layer growth.[24,32,38] The Cu thus deposits with lower energy on the substrate further inducing defects and yielding a deteriorated crystallinity. SEM images in Fig. S3, show that an increase in deposition pressure results in the particles becoming more stacked and agglomerated, as was observed in previous literature.[36,38] In this regime, higher diffusion rate and atom mobility result in a more densely stacked surface.

Next, we compared the different sputter rates in Fig. 1C, the crystallinity of the characteristic Cu_3N peaks are similar with varying sputter rate. A higher rate will result in more material deposited on the carbon substrate, as evidenced by the ICP–MS result on Cu loading (Table S1), consequently, the intensity of the Cu_3N peaks increase. Furthermore, SEM images (Fig. S4) reveal an increase in mean average size was detected from 394 nm ± 47 nm for 1 Å s^{-1} to 516 nm ± 35 nm for 10 Å s^{-1}. This can be attributed to a faster growth rate and less nucleation under the latter conditions.[32]

Next, contact angles were measured on the $Cu_{1-x}N_x$ coated GDLs for each sample. Table 1 (Fig. S5–S7, for pictures) shows that the contact angle lowers with r_{N2}, as the nitrogen content

Table 1 An overview of the measured contact angles for the different prepared samples. The contact angle was measured with a droplet of water onto the catalyst coated GDL

Sample	Contact angle (°)
r = 0	106.16
r = 0.25	85.4
r = 0.5	86.6
r = 0.75	63.1
P = 6	86.6
P = 10.5	57.5
P = 15	47.7
SR = 1	102.4
SR = 4	86.6
SR = 7	74.3
SR = 10	65.2

increases, Cu_3N has a higher contribution, which is intrinsically more hydrophilic than Cu, due to its higher polarity. A higher P makes the surface more amorphous as evidenced by XRD, which will reduce the contact angle further. Finally, a lower SR results in reduced Cu loadings; therefore, exposing more of the hydrophobic carbon-based GDL to the water droplet as such yielding a higher contact angle for the lowest SR of 1 Å s^{-1}.

Electrochemical results

The different $Cu_{1-x}N_x$ films were then tested for their performance towards the eCO_2R in a flow-by (Fig. S1) configuration at an industrial current density of −150 mA cm^{-2}, which was chosen based on our previous study on Cu films towards C_{2+} products.[13] A higher current induces faster degradation, whereas a lower current results in the formation of more C_1 products.[39] In Fig. 2A, the effect of the r_{N2} factor on the product distribution towards the various reduction products was studied. In all cases, FE_{C2+} remained similar at approximately 72%, with ethylene (44%) and ethanol (21%) as the main C_{2+} products. As for a typical Cu-based catalyst several other products such as $CO/HCOO^-/CH_4/C_3H_5OH$ were detected albeit with efficiencies below 10%.[40] Importantly, the parasitic hydrogen evolution reaction (HER) remained below 8% in all cases. While comparable FE were obtained in the presence and absence of N_2, there was a notable difference between the measured cathodic potential (Fig. 2B) between pure Cu and $Cu_{1-x}N_x$ attributed to the compositional differences. For a pure Cu film, the cathodic potential varies between −1.9 and −2.1 V *vs.* RHE, whilst for r_{N2} = 0.5 the potential remains between −1.3 and −1.4 V *vs.* RHE, a remarkable difference of 600 mV, which translates in a significant difference in energy input that is needed to perform eCO_2R at the given current density. Upon calculating the cathodic energy efficiency (cEE) a clear improvement is thus also observed from 15.8% for ethylene at r_{N2} = 0 to 20% at r_{N2} = 0.5, which is, when comparing to other reported catalysts for C_2, a remarkable improvement (Table S2).[12,41–43]

Next, the pressure (Fig. 2C and D) had a more profound effect on C_{2+} selectivity as it dropped from 72% to around 65% upon increasing the pressure above 6 μbar, with a significant increase in the production of $HCOO^-$ as a consequence (up to 16% for P = 15 μbar). This may be explained by the agglomerated particles that form at these higher P. Since, they have a higher coordination number, they can be expected to be less active for C_{2+} as they have lower surface energies.[44] Additionally, the measured potential for P = 15 μbar fluctuated more and reached values as high as −2.1 V *vs.* RHE, compared to −1.4 V for P = 6 μbar, indicating that stability and activity suffered as well upon increasing the pressure. The significant decrease in contact angle for high pressure (from 86° to 47°) alters the surface tension of water so that molecules can penetrate more easily, enhancing the HER, this seems to be most outspoken when increasing the pressure.[45]

When increasing the SR (1–4–7–10 Å s^{-1}), only a small impact on the C_{2+} formation (67–72–70–66%) was observed, highlighted by the simultaneous increase in C_1 and HER (10%) (Fig. 2E/F). A higher SR (> 4 Å s^{-1}) showed a steady increase in CO and HER, while the potential increased to −1.5 V *vs.* RHE for SR = 7 Å s^{-1}, and −1.7 V *vs.* RHE for SR = 10 Å s^{-1}. At these higher SR, the particles are more amorphous, making them less active. The lowest SR of 1 Å s^{-1} nevertheless had the highest potential (−2.7 V *vs.* Ag/AgCl), and a possible explanation is the low amount of deposited catalyst rendering less active sites enabling HER and inhibiting C–C coupling.

The $Cu_{1-x}N_x$ films prepared by magnetron sputtering clearly provide promising performance as electrocatalysts for CO_2 reduction. To further explain the improvement in activity (*i.e.*, higher EE) from pure Cu, we estimated the electrochemical active surface area (EASA) of all the samples by determining the double layer capacitance (C_{dl}) (Fig. S8 & Table S3). From the summarized results in Table S3, it can be concluded that the optimal sample (r_{N2} = 0.5; SR = 4 Å s^{-1}; P = 6 μbar) possesses the highest EASA value of 4.08 mF (as it is an indication of roughness), and thus is most active towards eCO_2R which explains why it reaches the highest EE value. A general trend among all catalysts is found that for higher C_{dl} values, improved energy efficiencies are observed. This observation suggests that the limited differences between the nitrogen containing samples are driven by their difference in the calculated active surface area (EASA). For instance, the extrapolated C_{dl} for r_{N2} = 0.50 has the highest value at 4.08 mF, compared to 3.8 mF for r_{N2} = 0.75, resulting in minor cEE differences between these two samples.

The (non-iR corrected) cathodic EE was then calculated for all samples for ethylene and ethanol, the two major products, and summarized in Table S3. Clearly, a maximum $EE_{C_2H_4}$ of 20% is reached for the sample configuration of r_{N2} = 0.5, SR = 4 Å s^{-1}, and an operational pressure of 6 μbar. Furthermore, the partial mass activity (mA mg^{-1}) for ethylene was calculated (Figu. S9), and a clear improvement from 193.2 mA mg^{-1} to 230.2 mA mg^{-1} was observed from pure Cu to $Cu_{0.84}N_{0.16}$ (r_{N2} = 0.5). This clearly highlights the advantage and novelty of using $Cu_{1-x}N_x$ film as a more efficient electrocatalyst when compared to the more commonly used Cu film, as the EE and mass activity improved significantly. In Table S2, a summary of recent Cu-based catalysts for C_{2+} production is given. Without iR correction, our material either equals or outperforms several

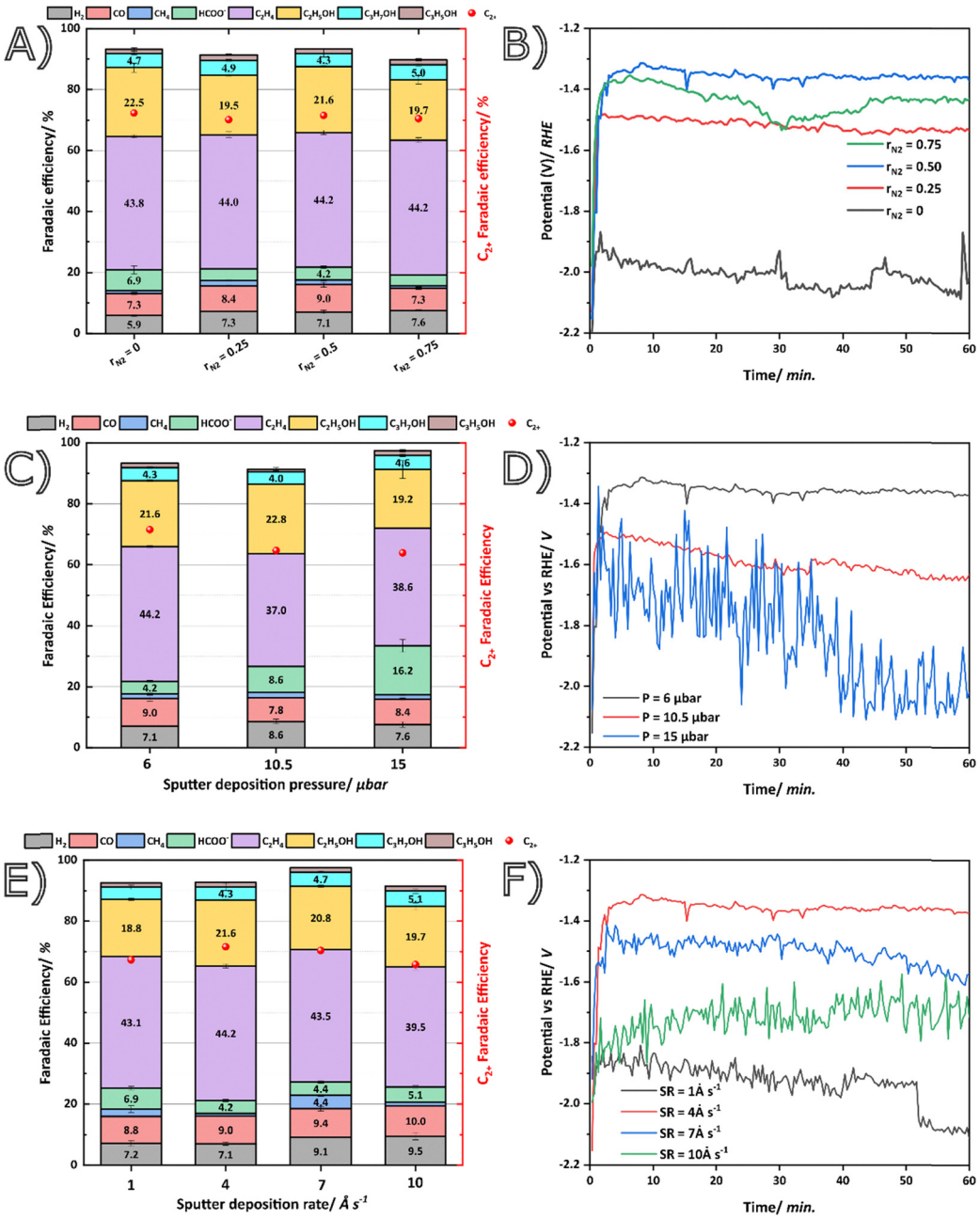

Fig. 2 The product distribution in terms of faradaic efficiency for the different products, and the recorded working electrode potential in RHE are given. Measurements were done in a flow-by configuration with 0.5 M $KHCO_3$ as catholyte, and 15 sccm of CO_2, chronopotentiometry analysis was done at −150 mA cm^{-2} and repeated three times for reproducibility. The results are presented for the parameters under investigation, (A) and (B) the varying r_{N2} values, (C) and (D) the different sputter deposition pressures in μbar, and (E) and (F) for the sputter deposition rates.

other reported studies in terms of EE, however, if iR contribution is applied, a total $EE_{C_2H_4}$ of 28% is found, further showing that our material is better than most previously reported Cu nitride based materials (Table S2). Furthermore, although the FEs might be comparable, emphasis on the high mass activity (due to low Cu loading) for ethylene is highlighted. In most cases, a higher mass activity is observed due to the sputtering fabrication method requiring low Cu loadings (<1 mg cm^{-2}). Magnetron sputtering thus allows for facile tuning of properties, whilst providing a rapid, uniform, and scalable fabrication strategy (up to ± 1 m^2) making this an optimal alternative for traditional, and complex synthesis methods even though they sometimes slightly outperform in terms of performance. For instance, Cu_3N-derived Cu nanowires (NWs) exhibit superior performance compared to our sample, achieving an $FE_{C_2H_4}$ of 66% and an $EE_{C_2H_4}$ of 35% albeit at lower current densities in a H-cell.[20] Nevertheless, the synthesis procedure entails the production of $Cu(OH)_2$ NWs, followed by nitridation in a tube furnace, and ultimately, partial electrochemical reduction to Cu NWs. Evidently, this method involves a complex fabrication

process that poses challenges for scaling to quantities relevant for industrial applications.

To conclude, the higher EE with $Cu_{1-x}N_x$ as opposed to metallic Cu can be explained as follows. First, the distinct anti-ReO_3 crystal structure that yields interstitial sites filled with Cu (as highlighted by the EDX) and Cu domains, increases the conductivity and stability of Cu^+ due to the presence of residual nitrogen (as supported by *ex situ* XRD analysis). Secondly, the greater interatomic distances (3.817 > 3.615 Å)[23] between Cu–Cu atoms can help in stabilizing certain intermediates by reducing the energy barrier and facilitating better adsorption and improved cell potentials. Finally, the significant charge density of N^{3-} contributes in maintaining the more active Cu^+ species, further contributing to the increased cEE.

Finally, we investigated the initial stability of the optimal $Cu_{1-x}N_x$ films (for r_{N2} = 0.50, SR = 4 Å s^{-1} and P = 6 μbar) and compared it to pure Cu. From Fig. 3A, similar potential trends are seen over the course of the experiment, as before, with r_{N2} = 0.50 a higher energy efficiency was reached due to a difference of ± 600 mV in the measured working potential. With respect to the ethylene efficiency over time (Fig. 3B), r_{N2} = 0.50 clearly achieves improved stability as the ethylene is still at 20% after 4 hours, whereas, for pure Cu the ethylene FE has dropped to zero. Therefore, it seems that $Cu_{0.84}N_{0.16}$ can retain higher production rates over extended duration and we believe this is due to the more defined crystal structure. During operation, sputtered metallic Cu reorganize into channel-like structures that allow enhanced water penetration.[13] A similar mechanism occurs with r_{N2} = 0.50, however, the initial nitrogen incorporation likely influences activation by stabilizing Cu^+, similar to the case of oxide-derived Cu.

Chronoamperometry at −0.5 V *vs.* Ag/AgCl (the potential at which Cu^+ reduces) was run until the current reached approximately zero (in 1 M K_2SO_4). After integrating the resulting curves (Fig. S10), we can calculate the amount of charge (C) required for reduction (when current reaches zero), which is significantly higher for r_{N2} = 0.50 (at 62.67 mC) than for Cu (38.5 mC), indicating prolonged Cu^+ retention, furthermore, the XRD (Fig. S11) of the spent sample shows some Cu_3N peaks, proving the presence of residual nitrogen which helps in stabilizing the catalyst. Although these initials experiments indicate another advantage of utilizing $Cu_{0.84}N_{0.16}$, stability is not solely related to the catalyst, but also to the system. Controlling the differential pressure[46] to limit flooding effects, operating under pulsations to counteract surface reconstructions,[21] flow cell setup,[47] and substrates effects such as a pure PTFE substrate that hinders salt precipitation,[48] are all determining factors that heavily impact stability, which is not the main aim of this work and also the reason why longer testing was not performed. The main aim is to point out the benefits of utilizing nitrogen during reactive sputtering over pure Cu as electrocatalyst for the CO_2 reduction reaction.

In this study, we have proven that the application of sputtered $Cu_{1-x}N_x$ films can be expanded to the field of CO_2 electrolysis, whilst accomplishing similar FEs, the energy input can be significantly improved compared to typical pure Cu films. As previously mentioned, the increase in the mass activity due to relatively low Cu loadings (<400 μg cm^{-2}) is

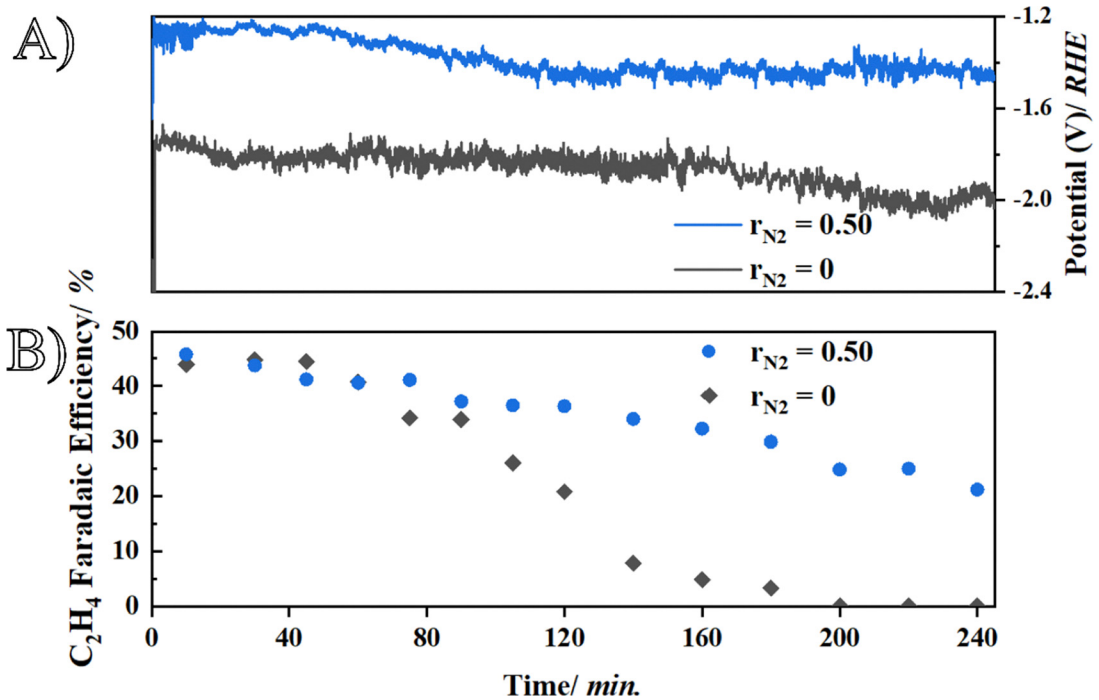

Fig. 3 $Cu_{1-x}N_x$ (r_{N2} = 0.50, P = 6 μbar, SR = 4 Å s^{-1}) and Cu (r_{N2} = 0, P = 6 μbar, SR = 4 Å s^{-1}) films were subjected to operational stability for 4 hours at −150 mA cm^{-2}. In (A) we plotted the measured working potential *vs.* RHE/V over time, and subsequently added the (B) ethylene efficiency over time for both samples.

another advantage of this cost – effective and scalable alternative. Therefore, we believe that $Cu_{1-x}N_x$ thin films have potential to be used as promising catalysts for the CO_2 reduction reaction, especially given there is still a lot of room for improvement of this system both in terms of efficiency and of stability.

Conclusions

In this study, we employed physical vapor deposition *via* magnetron sputtering to fabricate $Cu_{1-x}N_x$ thin films under varying operational parameters, including the r_{N2} ratio, sputter pressure, and sputter rate, and investigated their structural characteristics. These films were explored, for the first time, as electrocatalysts for the CO_2 reduction to multi-carbon products in a flow-by electrolyzer, and compared with well-studied metallic Cu films. From the results, we determined that $Cu_{1-x}N_x$ tends to generate equally remarkable faradaic efficiencies for ethylene (44%) and ethanol (21%) as compared to Cu. Notably, a significant enhancement in energy efficiency – from 15.8% to 20% – was observed for the optimized $Cu_{1-x}N_x$ sample (r_{N2} = 0.50, SR = 4 Å s^{-1}, P = 6 μbar) due to the differences in compositional effects enhancing stabilization of key intermediates and improving initial resistance of the system leading to higher energy efficiencies. Additionally, this straightforward, scalable and cost-effective synthesis allows for effective tuning of properties and has a large industrial relevance. This approach yields higher mass activity due to the reduced Cu loading required for ethylene production. The initial stability of $Cu_{0.84}N_{0.16}$ showed improvements compared to metallic Cu, as surface reconstructions are limited due to prolonged Cu^+ presence.

Author contributions

Mathias van der Veer: writing – original draft, conceptualization, investigation. Nick Daems: writing – review & editing, supervision. Pegie Cool: writing – review & editing, project administration, funding acquisition. Tom Breugelmans: riting – review & editing, project administration, funding acquisition.

Conflicts of interest

The authors report no conflict of interest.

Data availability

The (processed) data will be published and made openly and freely available through deposition in the Zenodo repository of the University of Antwerp and Applied Electrochemistry and Catalysis (ELCAT) Research Group. **https://zenodo.org/communities/uantwerp-elcat/**.

Supplementary information: detailed experimental methods; summary of deposition conditions, ICP-MS results, EDX results; literature review of various Cu-based catalysts; view of the flow cell; SEM images of $Cu_{1-x}N_x$ films prepared with different r_{N2} ratios; SEM images of $Cu_{1-x}N_x$ films prepared with different operational sputter pressure; SEM images of $Cu_{1-x}N_x$ films prepared with different sputter rates; contact angles of $Cu_{1-x}N_x$ films prepared with different r_{N2} ratios; contact angle of $Cu_{1-x}N_x$ films prepared with different operational pressure; contact angle of $Cu_{1-x}N_x$ films prepared with different sputter rate; cyclic voltammograms and the resulting linear fit for calculation of EASA data for all used $Cu_{1-x}N_x$ films; summary of our results with EE and Cdl; summary of partial mass activity; chronoamperometry with r_{N2} = 0, and r_{N2} = 0.50 at −0.5 V *vs*. Ag/AgCl; XRD pattern of r_{N2} sample after electrolysis. See DOI: **https://doi.org/10.1039/d5ey00246j**.

Acknowledgements

The authors acknowledge funding from the BOF-TOP project 2022–2025 (ID: 43950). We thank Karsten Heinz for the SEM measurements and Thomas Kenis/Max van Brusselen for configuration of the analytical equipment (GC-FID, GC-TCD, HPLC).

References

1 B. Obama, The irreversible momentum of clean energy, *Science*, 2017, **355**, 126–129.
2 M. van der Veer, N. Daems, P. Cool and T. Breugelmans, From batch to flow: the effect of pH, current, and the crystal facets of Cu_2O on electrochemical CO_2 reduction. Sustain, *Energy Fuels*, 2024, **8**, 2504–2518.
3 R. B. Sandberg, J. H. Montoya, K. Chan and J. K. Nørskov, CO–CO coupling on Cu facets: Coverage, strain and field effects, *Surf. Sci.*, 2016, **654**, 56–62.
4 A. A. Peterson, F. Abild-Pedersen, F. Studt, J. Rossmeisl and J. K. Nørskov, How copper catalyzes the electroreduction of carbon dioxide into hydrocarbon fuels, *Energy Environ. Sci.*, 2010, **3**, 1311–1315.
5 X. Nie, W. Luo, M. J. Janik and A. Asthagiri, Reaction mechanisms of CO_2 electrochemical reduction on Cu(1 1 1) determined with density functional theory, *J. Catal.*, 2014, **312**, 108–122.
6 S. Yousaf, I. Ahmad, M. Warsi and A. Ali, Engineering Strategies in Rational Design of Cu-Based Catalysts for Electrochemical CO_2 Reduction: From Doping of Elements to Defects creation, *Mater Adv.*, 2024, **5**, 7891–7978.
7 N. Daems, *et al.*, Steering Hydrocarbon Selectivity in CO_2 Electroreduction over Soft-Landed CuO_x Nanoparticle-Functionalized Gas Diffusion Electrodes, *ACS Appl. Mater. Interfaces*, 2022, **14**, 2691–2702.
8 M. Dauda, *et al.*, Electrochemical Reduction of CO_2: A Common Acetyl Path to Ethylene, Ethanol or Acetate, *J. Electrochem. Soc.*, 2024, **171**, 034501.
9 W. Huang, Oxide Nanocrystal Model Catalysts, *Acc. Chem. Res.*, 2016, **49**, 520–527, DOI: **10.1021/acs.accounts.5b00537**.
10 T. Möller, *et al.*, Electrocatalytic CO_2 Reduction on CuO_x Nanocubes: Tracking the Evolution of Chemical State,

Geometric Structure, and Catalytic Selectivity using Operando Spectroscopy, *Angew. Chem., Int. Ed.*, 2020, **59**, 17974–17983.
11 H. Tang, Y. Liu, Y. Zhou, Y. Qian and B. L. Lin, Boosting the Electroreduction of CO2 to Ethanol via the Synergistic Effect of Cu–Ag Bimetallic Catalysts, *ACS Appl. Energy Mater.*, 2022, **5**, 14045–14052.
12 M. Sassenburg, H. P. Iglesias van Montfort, N. Kolobov, W. A. Smith and T. Burdyny, Bulk Layering Effects of Ag and Cu for Tandem CO_2 Electrolysis, *ChemSusChem*, 2024, e202401769, DOI: 10.1002/CSSC.202401769.
13 M. Veer, N. van der, Daems, P. Cool and T. Breugelmans, Enhancing selectivity and stability in electrochemical CO_2 reduction using tailored sputtered CuAg electrodes, *Green Chem.*, 2025, **27**, 6039–6055.
14 Z. Zhang, *et al.*, Charge-Separated $Pd^{\delta-}$–$Cu^{\delta+}$ Atom Pairs Promote CO_2 Reduction to C2, *Nano Lett.*, 2023, **23**, 2312–2320.
15 Y. Yang, H. Fu, C. Xiao, X. Du and Z. Song, Efficient electrochemical CO_2 reduction to C^{2+} hydrocarbons on Zn-doped Cu films, *Appl. Surf. Sci.*, 2024, **646**, 158866.
16 J. Albo, M. Perfecto-Irigaray, G. Beobide and A. Irabien, Cu/Bi metal-organic framework-based systems for an enhanced electrochemical transformation of CO_2 to alcohols, *J. CO2 Util.*, 2019, **33**, 157–165.
17 C. T. Dinh, *et al.*, CO_2 electroreduction to ethylene via hydroxide-mediated copper catalysis at an abrupt interface, *Science*, 2018, **360**, 783–787.
18 Z. Yin, *et al.*, Cu_3N nanocubes for selective electrochemical reduction of CO_2 to ethylene, *Nano Lett.*, 2019, **19**, 8658–8663.
19 H. Wang, *et al.*, Cu_3N nanoparticles with both (100) and (111) facets for enhancing the selectivity and activity of CO_2 electroreduction to ethylene, *New J. Chem.*, 2022, **46**, 12523–12529.
20 Y. Mi, *et al.*, Selective Electroreduction of CO_2 to C_2 Products over Cu_3N-Derived Cu Nanowires, *ChemElectroChem*, 2019, **6**, 2393–2397.
21 J. Kok, J. de Ruiter, W. van der Stam and T. Burdyny, Interrogation of Oxidative Pulsed Methods for the Stabilization of Copper Electrodes for CO_2 Electrolysis, *J. Am. Chem. Soc.*, 2024, **146**(28), 19509–19520.
22 Z. Q. Liang, *et al.*, Copper-on-nitride enhances the stable electrosynthesis of multi-carbon products from CO_2, *Nat. Commun.*, 2018, **9**, 1–8.
23 A. Jiang, M. Qi and J. Xiao, Preparation, structure, properties, and application of copper nitride (Cu_3N) thin films: A review, *J. Mater. Sci. Technol.*, 2018, **34**, 1467–1473.
24 M. I. Rodríguez-Tapiador, *et al.*, Effect of N_2 concentration on structural, morphological, and optoelectronic properties of Cu_3N films fabricated by RF magnetron sputtering for photodetection applications, *Mater. Sci. Semicond. Process.*, 2025, **188**, 109176.
25 A. Razeghizadeh, M. Mahmoudi Ghalvandi, F. Sohilian and V. Rafee, The Effect of Substrate on Structural and Electrical Properties of Cu_3N Thin Film by DC Reactive Magnetron Sputtering, *Phys. Chem. Res.*, 2017, **5**, 497–504.
26 E. Márquez, *et al.*, Optical Properties of Reactive RF Magnetron Sputtered Polycrystalline Cu3N Thin Films Determined by UV/Visible/NIR Spectroscopic Ellipsometry: An Eco-Friendly Solar Light Absorber, *Coatings*, 2023, **13**, 1148.
27 S. Sakalley, *et al.*, Enhanced hydrogen gas sensing through the utilization of a hybrid nanostructure combining ZnO nanotubes and HiPIMS Cu_3N thin film, *Sens. Actuators, B*, 2024, **402**, 135107.
28 A. N. Fioretti, *et al.*, Understanding and control of bipolar self-doping in copper nitride, *J. Appl. Phys.*, 2016, **119**, 181508.
29 C. A. Figueira, G. Rosario, D. Pugliese, M. I. Rodríguez-Tapiador and S. Fernández, Effect of Argon on the Properties of Copper Nitride Fabricated by Magnetron Sputtering for the Next Generation of Solar Absorbers, *Materials*, 2022, **15**, 8973.
30 S. Majumder, *et al.*, Effect of N_2 gas fractions on improvement of structural, optical, and electrical properties of Cu_3N thin films deposited by reactive radio frequency magnetron sputtering, *J. Alloys Compd. Commun.*, 2025, **5**, 100049.
31 D. Depla and R. De Gryse, Target poisoning during reactive magnetron sputtering: Part I: the influence of ion implantation, *Surf. Coat. Technol.*, 2004, **183**, 184–189.
32 M. I. Rodríguez-Tapiador, *et al.*, Power effect on the properties of copper nitride films as solar absorber deposited in pure nitrogen atmosphere, *Appl. Res.*, 2022, **3**(1), 1–7.
33 J. T. Gudmundsson, A. Anders and A. von Keudell, Foundations of physical vapor deposition with plasma assistance, *Plasma Sources Sci. Technol.*, 2022, **31**, 083001.
34 A. K. Mukhopadhyay, M. A. Momin, A. Roy, S. C. Das and A. Majumdar, Optical and Electronic Structural Properties of Cu_3N Thin Films: A First-Principles Study (LDA + U), *ACS Omega*, 2020, **5**, 31918–31924.
35 D. M. Borsa and D. O. Boerma, Growth, structural and optical properties of Cu_3N films, *Surf. Sci.*, 2004, **548**, 95–105.
36 M. M. Islam and D. G. Georgiev, Stable stoichiometric copper nitride thin films via reactive sputtering, *Appl. Phys. A: Mater. Sci. Process.*, 2022, **128**, 1–11.
37 K. Joo Kim, J. Hyuk Kim and J. Hoon Kang, Structural and optical characterization of Cu3N films prepared by reactive RF magnetron sputtering, *J. Cryst. Growth*, 2001, **222**, 767–772.
38 Y. H. Chen, *et al.*, Enhanced Electrical Properties of Copper Nitride Films Deposited via High Power Impulse Magnetron Sputtering, *Nanomaterials*, 2022, **12**, 2814.
39 M. P. Schellekens, S. J. Raaijman, M. T. M. Koper and P. J. Corbett, Temperature-dependent selectivity for CO electroreduction on copper-based gas-diffusion electrodes at high current densities, *Chem. Eng. J.*, 2024, **483**, 149105.
40 Y. Hori, A. Murata and R. Takahashi, Formation of hydrocarbons in the electrochemical reduction of carbon dioxide at a copper electrode in aqueous solution, *J. Chem. Soc., Faraday Trans. 1*, 1989, **85**, 2309–2326.
41 F. Huq, *et al.*, Influence of the PTFE Membrane Thickness on the CO_2 Electroreduction Performance of Sputtered Cu-PTFE Gas Diffusion Electrodes, *ChemElectroChem*, 2022, **9**, e202101279.

42 Y. C. Li, *et al.*, Binding Site Diversity Promotes CO_2 Electroreduction to Ethanol, *J. Am. Chem. Soc.*, 2019, **141**, 8584–8591.
43 F. Jiao, *et al.*, Scalable gas diffusion electrode fabrication for electrochemical CO_2 reduction using physical vapor deposition methods, *ACS Appl. Mater. Interfaces*, 2022, **14**, 7731–7740.
44 C. Zhan, *et al.*, Key intermediates and Cu active sites for CO_2 electroreduction to ethylene and ethanol, *Nat. Energy*, 2024, **9**, 1485–1496.
45 E. Bormashenko and O. Gendelman, A generalized electrowetting equation: Its derivation and consequences, *Chem. Phys. Lett.*, 2014, **599**, 139–141.
46 A. Rossen, N. Daems, D. Choukroun and T. Breugelmans, Differential Pressure Across a Gas Diffusion Electrode Controls Efficiency of Liquid-Fed Electrolyzers for CO_2 Electroreduction at Elevated Temperatures, *ACS Sustainable Chem. Eng.*, 2024, **12**, 7935–7942.
47 B. Sahin, *et al.*, Fine-tuned combination of cell and electrode designs unlocks month-long stable low temperature Cu-based CO_2 electrolysis, *J. CO_2 Util.*, 2024, **82**, 102766.
48 S. Van Daele, *et al.*, Promoting CO_2 reduction in the presence of oxygen with polymer-based gas diffusion electrodes, *Chem. Catal.*, 2025, **5**, 101353.